

A soil water hysteresis model for fingered flow data

Yaping Liu,¹ J.-Yves Parlange, and Tammo S. Steenhuis

Department of Agricultural and Biological Engineering, Cornell University, Ithaca, New York

Randel Haverkamp

Institut de Mécanique de Grenoble, Grenoble, France

Abstract. Wetting and drying boundaries of a hysteresis loop were measured for fingered flow in a uniform sand, as well as drying scanning curves within the loop. The data are described by a soil water hysteresis model that uses a Brooks and Corey (1964) type main wetting boundary curve to predict the boundaries and scanning curves. The model requires as input parameters the bulk density, matric potential, water content at the two intersection points between the wetting and drying boundary curves, and one parameter obtained by curve fitting. The analysis is used to explain a fingered flow pattern in an uniform sand with different initial moisture contents.

Introduction

While water movement in unsaturated soils is commonly affected by hysteresis, this phenomenon is often masked by field heterogeneities. Hysteresis cannot be ignored when local, rather than average, soil properties are used, which arises in cases of fingered flow caused either by an unstable wetting [Glass *et al.*, 1989] or a point source with constant flux. The latter approximates a water distribution in the finger asymptotically identical to that obtained in unstable flow [Glass *et al.*, 1987; Liu *et al.*, 1993; Selker *et al.*, 1992].

Poulovassilis [1962] presented the first applications of independent domain theory to soils in the description of soil water hysteresis. A simple model that is partly based on the same theory was proposed by Parlange [1976, 1980]. This model predicts scanning curves within a hysteretic loop using data from only one boundary and leads to elementary analytical expressions when the main wetting boundary is described by the Brooks and Corey [1964] equation. The model was used by Haverkamp and Parlange [1986] and by Hogarth *et al.* [1988] to derive first-order scanning curves. It is generalized here for the analytical derivations of scanning curves of any order starting with the main wetting boundary, which is obtained by simultaneously measuring the moisture content and matric potential for infiltration into an initially dry soil. First-order scanning curves originate from the main boundaries. Secondary curves originate from primary curves, etc. If we denote by $\Theta(h)$ the volumetric water content as a function of the matric potential h , and subscripts w and d indicate measurements on a wetting or drying curve, respectively, then the model of Parlange [1976, 1980] postulates that a drying curve issued from any wetting curve is given by

$$\Theta_d(h, h_{n+1}) = \Theta_w(h, h_n) - [h - h_{n+1}] \frac{d\Theta_w(h, h_n)}{dh} \quad (1)$$

where $\Theta_w(h, h_n)$ is a wetting curve of n th order and $\Theta_d(h, h_{n+1})$ is a drying curve of order $(n + 1)$ issued from $\Theta_w(h, h_n)$ at $h = h_{n+1}$. (Note that the subscript of the last h is equal to the order of the curve.) While $d\Theta_w(h, h_n)/dh$ in (1) is dependent on h , near saturation $d\Theta_w(h, h_n)/dh$ is constant up to the air entry value. If $d\Theta_w(h, h_n)/dh$ is constant, differentiation of (1) shows that $d\Theta_d(h, h_{n+1})/dh = 0$ over that interval; that is, $\Theta_d(h, h_{n+1})$ is also constant.

A wetting curve, $\Theta_w(h, h_{n+2})$, issued from an order $(n + 1)$ drying curve, $\Theta_d(h, h_{n+1})$, is of the order of $(n + 2)$ and can be described in the most general terms by [Parlange, 1976]

$$\Theta_w(h, h_{n+2}) = \Theta_w(h, h_n) - [h - h_{n+1}] \frac{d\Theta_w(h, h_n)}{dh_{n+2}} \quad (2)$$

where $d\Theta_w(h, h_n)/dh_{n+2}$ is the tangent to the wetting curve of the n th order evaluated at $h = h_{n+2}$. The point (h_{n+2}, θ_{n+2}) represents the location where the wetting curve of the order of $(n + 2)$ originates from the drying curve of the $(n + 1)$ th order. Equation (2) requires that any wetting curve of the order of $(n + 2)$ originating from a $(n + 1)$ th-order drying curve must return to the point where the $(n + 1)$ th-order drying curve started on the n th-order wetting curve [Parlange, 1976].

The use of (1) and (2) is illustrated with a specific example related to an experiment discussed later (Figure 1). The moisture characteristic curves can be separated into main (or zero-order), first-order, second-order, third-order, etc.

The main wetting curve ($n = 0$), $\Theta_w(h, h_0)$, begins at $\theta = 0$ and $h = -\infty$ and ends at $\theta = \varepsilon$, and $h = 0$, where ε is the soil porosity. It is curved (equation (1)) from the point $(-\infty, 0)$ to the air entry value, h_{ae} , at which point $\theta = \theta_{Mae}$. Following Hogarth *et al.* [1988] the curved portion of the line can be described by the Brooks and Corey [1964] equation of the form

$$\frac{\Theta_w(h, h_0)}{\theta_{Mae}} = \left[\frac{h_{ae}}{h} \right]^\lambda \quad h \leq h_{ae} \quad (3)$$

where λ is the pore index associated with soil structure and packing conditions. Following Haverkamp and Parlange [1986], the line from (h_{ae}, θ_{Mae}) that passes through the point $(0, \varepsilon)$ is straight and tangent to equation (3) at (h_{ae}, θ_{Mae}) . This results in [Haverkamp and Parlange, 1986]

¹Now at Department of Land, Air, and Water Resources, University of California, Davis.

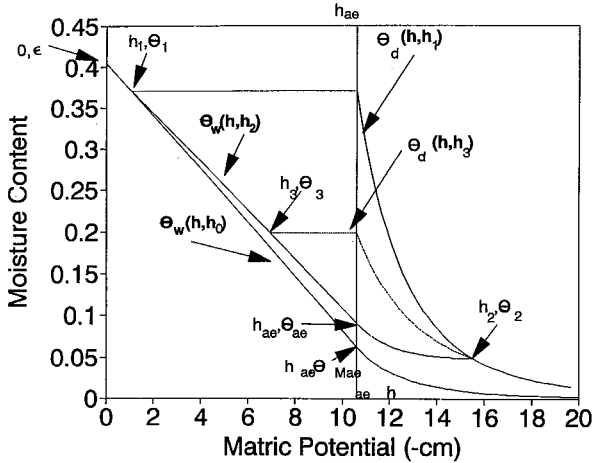


Figure 1. Schematic diagram of wetting and drying branches of the soil moisture characteristic curve. $\Theta_w(h, h_0)$ is the main wetting curve, $\Theta_d(h, h_1)$ is a first-order drying curve issued from h_1, θ_1 on $\Theta_w(h, h_0)$, $\Theta_w(h, h_2)$ is the secondary wetting curve starting at h_2, θ_2 on $\Theta_d(h, h_1)$, $\Theta_d(h, h_3)$ is a third-order drying curve, and h_{ae} is the matric potential at the air entry value.

$$\theta_{Mae} = \frac{\varepsilon}{1 + \lambda} \quad (4)$$

where the porosity ε can be calculated directly from the bulk density assuming that there is no air inclusion.

The first-order drying curve $\Theta_d(h, h_1)$ originates at the point (h_1, θ_1) on the main wetting curve and is described by (1) with $n = 0$. The moisture content on the drying curve remains equal to θ_1 from h_1 until h_{ae} . The remainder is described by substituting (3) and (4) into (1) and differentiating:

$$\frac{\Theta_d(h, h_1) - \theta_1}{\theta_{Mae}} = \left[1 + \lambda - \lambda \frac{h_1}{h} \right] \left[\frac{h_{ae}}{h} \right]^\lambda \quad (5)$$

The second-order wetting curve $\Theta_w(h, h_2)$ originates from any point (h_2, θ_2) (Figure 1) on the first-order drying curve $\Theta_d(h, h_1)$. The second-order wetting curve returns to the point (h_1, θ_1) . By substituting the zero-order wetting curve (equation (3)) into (2), differentiating, and evaluating it at h_2 , we find that for $h \leq h_{ae}$,

$$\frac{\Theta_w(h, h_2) - \theta_2}{\theta_{Mae}} = \left[\frac{h_{ae}}{h} \right]^\lambda + \lambda \frac{h}{h_2} \left[\frac{h_{ae}}{h_2} \right]^\lambda - \left[\frac{h_{ae}}{h_2} \right]^\lambda [1 + \lambda] \quad (6)$$

Equation (6) shows the interesting property that as long as the point (h_2, θ_2) is known, the drying curve originating at h_1 does not explicitly affect the wetting curve. That is, all drying curves of increasing order will lead to the same wetting curve described by (6), as long as they pass through (h_2, θ_2) .

The derivative $d\Theta_w(h, h_2)/dh$ (also called the specific capacity) obtained from (6) evaluated at the air entry pressure h_{ae} is equal to the slope of the straight part of the wetting curve for $h > h_{ae}$ [Hogarth et al., 1988], or

$$\frac{d\Theta_w(h, h_2)}{dh_{ae}} = \frac{\lambda \theta_{Mae}}{h_{ae}} \left[-1 + \left[\frac{h_{ae}}{h_2} \right]^{\lambda+1} \right] \quad (7)$$

and the equation for the straight line can be found as

$$\Theta_w(h, h_2) - \theta_{ae} = (h - h_{ae}) \frac{d\Theta_w(h, h_2)}{dh_{ae}} \quad (8)$$

The value of θ_{ae} is obtained by applying (6) at $h = h_{ae}$, or,

$$\frac{\theta_{ae} - \theta_2}{\theta_{Mae}} = 1 + \left[\frac{h_{ae}}{h_2} \right]^\lambda \left[\lambda \frac{h_{ae}}{h_2} - 1 - \lambda \right] \quad (9)$$

where (h_{ae}, θ_{ae}) is the point on the wetting curve where the straight line meets the curved section (Figure 1).

A drying curve originating from the second-order wetting curve is of the third order. If we call the originating point (h_3, θ_3) , then the third-order drying curve is indicated by $\Theta_d(h, h_3)$. The drying curve for $h \leq h_{ae}$ is found by substitution of (6) into (1) and differentiating:

$$\frac{\Theta_d(h, h_3) - \theta_2}{\theta_{Mae}} = \left[\frac{h_{ae}}{h} \right]^\lambda \left[1 + \lambda - \frac{h_3}{h} \lambda \right] - \left[\frac{h_{ae}}{h_2} \right]^\lambda \left[1 + \lambda - \lambda \frac{h_3}{h_2} \right] \quad (10)$$

As was noted above, the different order wetting curves should be the same. We see, indeed, that by substitution of (6) into (2) the derivative is zero when evaluated at h_2 , resulting in identical the fourth- and second-order wetting curves.

Fitting the Soil Moisture Characteristic Curves

The method for estimating boundary and scanning curves consists of the following procedure: First, collect a number (three or four) of drying curves of several orders that coalesce at the same point (h_2, θ_2) . This usually requires a fairly low θ_2 . Then check if their starting points are approximately along a straight line in a (h, θ) plot. Next an initial estimate of h_{ae} is obtained from drying curves, usually from a first-order drying curve with a large h_1 , that is, h_1 close to zero. Finally, obtain, as explained below, λ from the equation,

$$\frac{\theta_2}{\varepsilon} = \left[\frac{h_{ae}}{h_2} \right]^\lambda \left[1 - \frac{h_1 \lambda}{h_2 [1 + \lambda]} \right] \quad (11)$$

which results from evaluating (5) at $h = h_2$. The quantity h_1/h_2 in (11) is normally so small that its influence is small, if not negligible, so that an iterative procedure easily yields λ as follows. First, replace the bracket in (11) by 1 and obtain a first estimate of λ . Use this estimate to obtain a better value for the bracket and obtain a second estimate of λ . The procedure can be repeated at will but will converge very fast for small h_1/h_2 . Equation (4) then provides an estimate for θ_{Mae} , and equation (9) is used to find θ_{ae} . Finally, (5), (6), (7), (8), and (10) are used to predict all scanning curves.

Equation (7) can be used as a check of the original choice for h_{ae} by predicting the value of $d\Theta_w(h, h_2)/dh_{ae}$ (the derivative evaluated at h_{ae}) and comparing with the line formed by the observed starting points of the drying curves. If the predicted result is clearly incompatible with the observations, it will be necessary to adjust the initially selected value for h_{ae} . This is possible because in the Brooks and Corey law, h_{ae} is a curve-fitting parameter.

Experimental Illustration

Experiments were conducted in two-dimensional rectangular chambers with transparent sides. Two types of chambers

were used, short ($37 \times 18 \times 0.8$ cm), and long ($80 \times 51 \times 1$ cm). The chambers were filled with washed and oven-dried (80°C) white silica sand with grain diameters between 0.59 and 0.85 mm. Sand was poured into the chamber through an extension funnel on top of the chamber to assure uniform packing. The top 10 cm of sand was removed, resulting in a uniform bulk density of 1.58 g/cm^3 . Particle density was assumed to be 2.65 g/cm^3 . This results in a porosity of 0.404.

Two layers with different initial water contents were established within each chamber. The top half of sand in the chamber was kept dry, while the bottom half of sand was saturated with water through the bottom of the chamber. After saturation the bottom layer was allowed to drain until a uniform volumetric water content of $\theta_2 \sim 0.05$ and $h_2 \sim 15.5 \text{ cm} \pm 0.5$ was reached. The narrow range of particle sizes assures that the primary drying curve will yield h_1 near zero and that several distinct drying curves of higher order will occur. For most natural soils, λ is normally around 3 or less [Haverkamp and Parlange, 1986] but tends to increase for narrow particle size distributions, which is the case here.

In this experiment, matric potentials were measured using rapid-response tensiometers described by Selker et al. [1992]. Water contents were obtained by two different methods: A light visualization technique [Glass et al., 1989] was used in the long chamber, while a high-intensity X ray beam, which is more accurate in wet soils, was used in the short chamber [Liu et al., 1993]. In order to measure the moisture contents in both the top and bottom layers with X rays, the chamber had to move mechanically up and down, resulting in an interval of 10 s between measurements.

Dripping water at a rate of $10 \text{ cm}^3/\text{min}$ through a tube located just above the sand surface resulted in a finger which passed through both the initially dry and prewetted layers. Once steady state flow conditions were reached, the application of water was halted, and the finger was left to drain until (h_2, θ_2) was obtained. Water application resumed with the same flow rate of $10 \text{ cm}^3/\text{min}$ until a steady flow was reached throughout the chamber. This procedure was repeated three

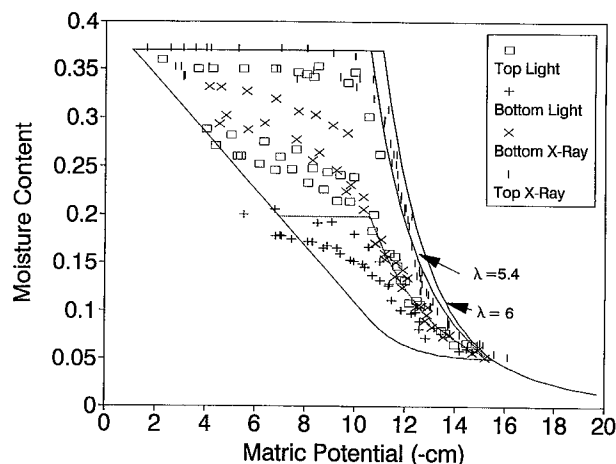


Figure 2. Measured drying curves (symbols) together with wetting and drying curves (lines) calculated with equations (5), (7), and (8). The wetting curve begins at $h_2 = -15.5$ and $\theta_2 = 0.05$. Two drying curves are issued from this wetting curve. The two solid lines start at $h_1 = -1.1$ and $\theta_1 = 0.37$, one with $h_{ae} = -10.6$, the other -11.1 . The dotted line starts at $h_1 = -7.1$ and $\theta_1 = 0.19$.

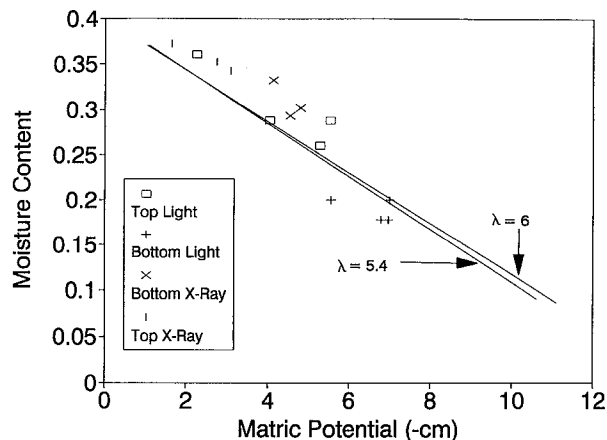


Figure 3. Measured starting points of the drying curves (symbols) and calculated straight line section of the wetting curve.

times before the sand in the chamber was removed, dried, and replaced. The short chamber yielded fingertips that were wetter (h_1 large) than fingertips in the longer chamber. More detail is provided by Liu et al. [1993, 1994].

Experimental results are shown in Figure 2. All drying curves converge near one point ($h_2 \approx -15.5$; $\theta_2 \approx 0.05$) and all starting points of the drying curves tend to lie on a straight line. While in principle, the wetting curve could be measured as the wet tip moves downward (velocity approximately 0.3 cm/s), the wetting normally occurs in less than 1 cm, so that wetting takes place in less than 3 s. The reaction time of our tensiometers is as high as 1 s, and thus measurement of wetting curves does not allow sufficient precision. This also results in uncertainty in the measured starting points of the drying curves, so that (7) should be used carefully.

Upper and lower estimates of air entry value from Figure 2 yield $-11.1 \leq h_{ae} \leq -10.6$. With $h_{ae} \approx -10.6$, equation (11) gives $\lambda \approx 5.5$ when the bracket is replaced by 1. A second iteration requires a knowledge of h_1 , which can be observed to be approximately -1 (Figure 2). Alternatively, because the starting point is on the main wetting curve, h_1 can also be estimated from

$$h_1 = \frac{\lambda + 1}{\lambda} h_{ae} \left(1 - \frac{\theta_1}{\epsilon} \right) \approx -1.1 \quad (12)$$

which is consistent with Figure 2. Equation (12) is based on finding the line for the straight segment of the main wetting curve through $(0, \epsilon)$. A second and subsequent iterations yield $\lambda \approx 5.4$. Repeating the process for $h_{ae} \approx -11.1$ gives an estimated $\lambda \approx 6.0$. The drying curves predicted by (10) are shown in Figure 2 for both values of λ .

Figure 3 presents experimentally determined initial water contents for the drying curves. The initial values were determined using the maximum observed moisture contents. Because of the longer time interval between measurements for the X ray system than for the light measurement, we find that as expected, the values obtained with the X ray system lie above the calculated line, while values using the light method are closer to the line. Using the point (h_1, θ_1) we can draw the corresponding linear segment with the constant slope estimated from (7). In the case $\lambda \approx 5.4$, $d\theta_w/dh \approx 0.029$, and for $\lambda \approx 6$, $d\theta_w/dh \approx 0.028$. In both cases, most of the points are

above the line, indicating that for these soils, λ has little effect on the wetting curve shape.

Equations (5), (6), (7), and (8) are used to predict the wetting curves and (10) the drying curves with $h_{ae} = -10.6$ cm, $\lambda \approx 5.4$, and the measured $(h_2, \theta_2) = (-15.5, 0.05)$. For $(h_1, \theta_1) = (-1.1, 0.37)$, Figure 2 again shows excellent agreement with the first drying curve. However, for drier starting points ($\theta_3 = 0.20$ with $h_3 = -7.0$), the prediction for θ close to θ_3 is flatter than observed, which holds for most soils with initially dry moisture contents, as was noted by Parlange [1976].

Conclusions

Measurements of drying curves for a sand are consistent with a theory of hysteresis based on a Brooks and Corey [1964] type wetting boundary that uses the bulk density and matric potential at the air entry value, h_{ae} .

We suggest estimating upper and lower values of h_{ae} from a drying curve as close as possible to saturation. For known end points $(h_2, \theta_2; h_1, \theta_1)$ the boundary of the loop and all scanning curves within the loop can be predicted using no additional parameters.

It is possible to evaluate the accuracy of the air entry values, because all starting points of the drying curves for $h_3 > h_{ae}$ should be on a predicted straight line.

Predicted scanning curves for dry initial moisture conditions display a flatter behavior near the starting point than was observed.

References

Brooks, R. H., and A. J. Corey, Hydraulic properties of porous media, *Hydrol. Pap. 3*, Colo. State Univ., Fort Collins, 1964.

Glass, R. J., J.-Y. Parlange, and T. S. Steenhuis, Water infiltration in layered soils where a fine textured layer overlays a coarse sand, in *Infiltration Development and Application, Proceedings of the International Conference on Infiltration Development and Application*, edited by Y. S. Fok, pp. 66–81, Univ. of Hawaii, Honolulu, 1987.

Glass, R. J., J.-Y. Parlange, and T. S. Steenhuis, Mechanism for finger persistence in homogeneous unsaturated, porous media: Theory and verification, *Soil Sci.*, 148(1), 60–70, 1989.

Haverkamp, R., and J.-Y. Parlange, Predicting the water-retention curve from particle-size distribution, 1, Sandy soils without organic matter, *Soil Sci.*, 142(6), 325–339, 1986.

Hogarth, W. L., J. Hopmans, J.-Y. Parlange, and R. Haverkamp, Application of a simple soil-water hysteresis model, *J. Hydrol.*, 98, 21–29, 1988.

Liu, Y., B. R. Bierck, J. S. Selker, T. S. Steenhuis, and J.-Y. Parlange, High-intensity X-ray and tensiometry measurements in rapidly changing preferential flow fields, *Soil Sci. Soc. Am. J.*, 57, 1188–1192, 1993.

Liu, Y., T. S. Steenhuis, and J.-Y. Parlange, Closed form solution for finger width in sandy soils at different water contents, *Water Resour. Res.*, 30(4), 949–952, 1994.

Parlange, J.-Y., Capillary hysteresis and the relationship between drying and wetting curves, *Water Resour. Res.*, 12(2), 224–228, 1976.

Parlange, J.-Y., Water transport in soils, *Annu. Rev. Fluid Mech.*, 12, 77–102, 1980.

Poulovassilis, A., Hysteresis of pore water, An application on the concept of independent domain, *Soil Sci.*, 93(6), 405–412, 1962.

Selker, J. S., J.-Y. Parlange, and T. S. Steenhuis, Fingering flow in two dimensions, 2, Predicting finger moisture profile and measure of conductivity, *Water Resour. Res.*, 28(9), 2523–2528, 1992.

R. Haverkamp, Institut de Mécanique de Grenoble, Domaine Universitaire, Grenoble Cedex 38401, France.

Y. Liu, Department of Land, Air, and Water Resources, University of California, Davis, CA 95616-8628.

J.-Y. Parlange and T. S. Steenhuis, Department of Agricultural and Biological Engineering, Cornell University, Ithaca, NY 14853-5701.

(Received January 31, 1995; revised May 1, 1995; accepted May 24, 1995.)